Supplementary Information (SI) for ChemComm.

ELECTRONIC SUPPLEMENTARY INFORMATION

Evaluating CO_2-to-Formic Acid Electrocatalysts in Different Device Configurations

Thuy-Duong Nguyen-Phan,[1]* James E. Ellis,[1,2] Bret H. Howard,[1] and Douglas R. Kauffman[1]*

[1] National Energy Technology Laboratory, 626 Cochran Mill Road, Pittsburgh, PA 15236, USA

[2] NETL Support Contractor, 626 Cochran Mill Road, Pittsburgh, PA 15236, USA

*Corresponding authors:

ThuyDuong.NguyenPhan@netl.doe.gov

Douglas.Kauffman@netl.doe.gov

1. Chemicals

Bi_2O_3 nanopowder (90-210 nm particle size), In_2O_3 nanopowder (<100 nm particle size), and SnO_2 nanopowder (≤100 nm average particle size) were purchased from Sigma-Aldrich and used as received without further purification.

2. Materials characterization

Scanning electron microscopy (SEM) imaging was performed on a FEI Quanta 600F microscope operated at 20 kV equipped with an energy-dispersive X-ray (EDX) and elemental mapping. X-ray powder diffraction (XRD) patterns were collected on a Malvern Panalytical Empyrean X-ray diffractometer using CuKα radiation ($\lambda = 1.5418$ Å).

3. Electrode fabrication

The ink solution containing 30 mg of nanopowder catalysts, 30 mg of Vulcan VC-X72 carbon black (Cabot), and 530 μL of Nafion 117 solution (5 wt%, Sigma) were dispersed in a mixture of 5 mL deionized water and 1.97 mL of isopropanol under sonication. For H-cell test, the working electrodes were prepared by drop-casting the catalyst ink onto 10% polytetrafluoroethylene (PTFE) treated Toray carbon paper (TGP-H-60, 0.2±0.05 mm thickness, Alfa Aesar). The mass loadings of electrode were kept at 8.6±0.1 mg_{ink}/cm_{geo}^2 (geometric area of 0.075±0.005 cm^2). For GDE half-cell and full cell tests, the 2.5 cm x 2.5 cm GDE electrodes were prepared by air brushing the ink onto 30% polytetrafluoroethylene (PTFE) treated Toray carbon paper (TGP-H-120, 0.37 mm thickness, Fuel Cell Store) on 80 °C hot plate. The mass loadings were kept at 3.2±0.2 mg_{ink}/cm_{geo}^2. After catalyst deposition, the GDE cathodes were sintered at 120 °C to increase adhesion and remove any leftover solvent.

4. Electrochemical CO_2 reduction evaluation

H-cell measurements: CO_2R measurements in an H-cell were conducted using a BioLogic SP-300 potentiostat and a gas-tight, two-compartment H-cell separated by a Nafion 117 proton exchange membrane. A Pt mesh and Ag/AgCl (saturated NaCl, BASi) were used as the counter and reference electrodes, respectively. 60 mL of aqueous 0.4 M K_2SO_4 catholyte (99.99%, Sigma) was continuously fed with high-purity CO_2 (Butler Gas, 99.999%) at a flow rate of 20 mL/min under vigorous stirring for at least 20 min prior to each test and during all the experiments. All applied potentials were reported against the reversible hydrogen electrode (RHE), and the uncompensated ohmic resistance obtained by conducting electrochemical impedance spectroscopy at each cathode potential. The cathode voltage was automatically corrected at 85% iR_u-correction using the instrument software and then manually corrected additional 15% to obtained 100% iR_u-drop correction. Chronoamperometric (current *vs.* time) measurements were performed for 30 min at each applied potential between -0.6 V to -1.4 V *vs.* RHE.

Half-cell and full-cell device measurements: The chronopotentiometry (potential *vs.* time) measurements were performed at several applied currents using BioLogic SP-150e potentiostat and 20A/20V booster. A formic acid electrolyzer cell (Dioxide Materials) was assembled with a 3 cm x 3 cm IrO_2-based GDE anode (Dioxide Materials), a 4 cm x 4 cm N-324 Nafion-based cation exchange membrane (Chemours), a polycarbonate central flow chamber filled with quartz wool (1.6 mm thick, 1 mL volume), and a GDE cathode fabricated above. Two peristaltic pumps deliver deionized water anolyte (4mL/min) and aqueous 0.4 M K_2SO_4 catholyte to the central chamber (4 mL/min), respectively. Dry CO_2 (100 mL/min) was fed to the cathode side and the cell was operated at room temperature for all experiments. In half-cell experiment, a mini hydrogen reference electrode (Mini-HydroFlex, Gaskatel) was inserted into a custom-built, 3D printed central flow chamber (3 mm thickness, 1.875 mL volume) to record cathodic potential against the RHE. The cathodic potentials were manually 100% iR_u-corrected with the uncompensated resistance obtained by electrochemical impedance spectroscopy at each applied current.

Product quantification: The gas and liquid products were collected in all testing devices every 30 min or 1 h at each potential or current. The gas products were collected in Tedlar gas-tight bags (Supelco) and analyzed by Shimadzu gas chromatography equipped with jetanizer, thermal conductivity and flame ionization detectors. Liquid products were first filtered with 0.22 μm PTFE syringe filters, diluted with deionized water, and quantified by Shimadzu liquid chromatography using 5 mM aqueous H_2SO_4 mobile phase, Aminex HPX-

87H column (Bio-Rad), and refractive index and photodiode array detectors. All the current densities in this work were normalized to the geometric area of the electrodes.

The calculation of Faradaic efficiency (FE, %), partial current density ($j_{product}$, mA/cm^2), and energy efficiency (EE, %) for each product is described below:

Equation S1: $FE = \frac{z * F * n}{I * t} = \frac{z * F * n}{Q}$, where $z = 2$ is the number of electrons involved in the reaction, F represents Faraday's constant (96485 C/mole); n is the moles of product; I is the total current during the sampling period; t is the sampling period; and $Q = I * t$ is total charge in Coulombs passed through the electrode during the sampling period.

Equation S2: $j_{product} = FE \cdot j_{total}$

Equation S3: $EE = \frac{E_{OER}^{0} - E_{CO2R}^{0}}{E_{cell}} * FE_{formic\ acid}$, where E^{o}_{OER} is the standard thermodynamic potential for oxygen evolution reaction (1.23 V), E^{o}_{CO2R} is the standard thermodynamic potential for CO_2 reduction to formic acid (-0.199 V), and E_{cell} is the measured full cell voltage.

5. Supporting figures

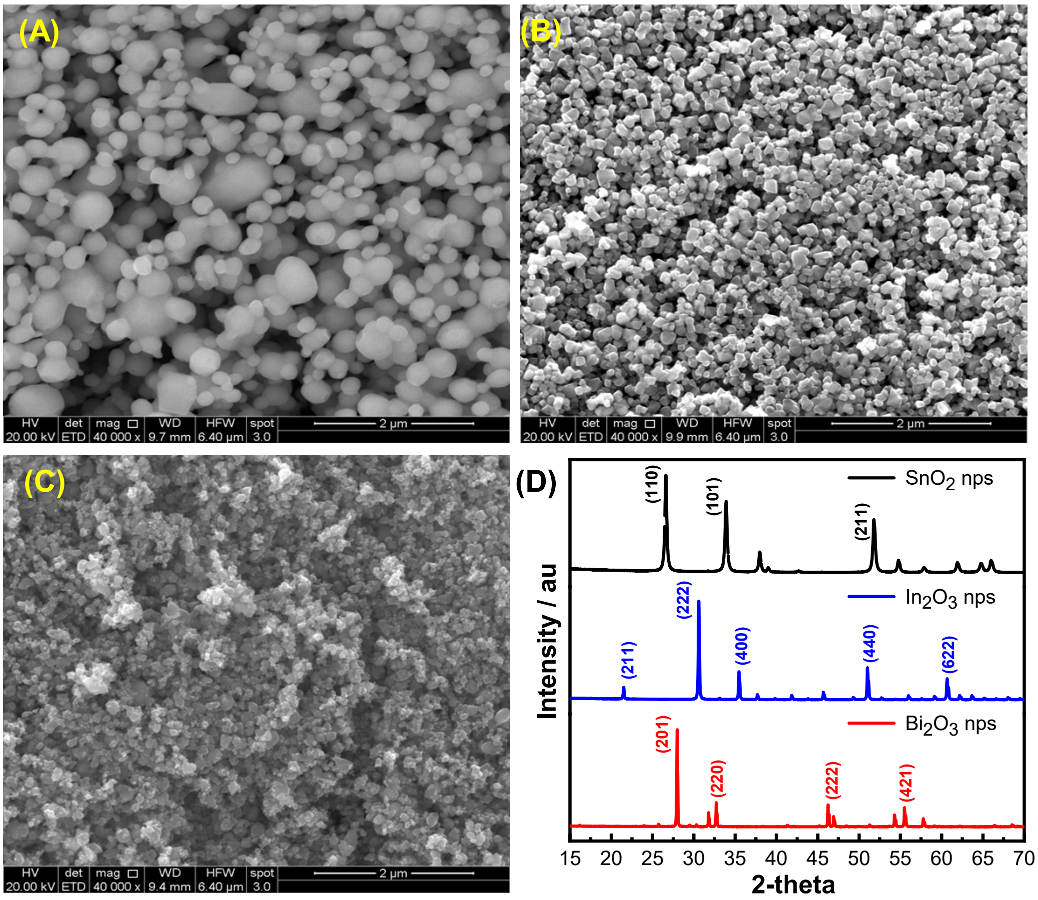

Figure S1. SEM images of (A) Bi_2O_3, (B) In_2O_3, and (C) SnO_2 nanoparticles before electrocatalytic CO_2R. (D) XRD pattern of three powder catalysts.

Figure S2. Images of (A) H-cell, (B) GDE half-cell with reference electrode integration, and (C) full single-gap electrolyzer cell for CO_2 electrolysis testing in this work. Half-cell and full cell were purchased from Dioxide Materials.

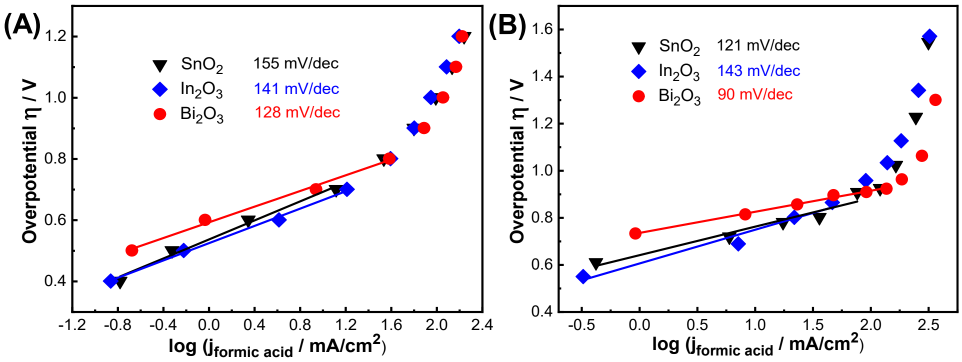

Figure S3. Tafel plots for Bi, Sn, and In oxide catalysts in (A) aqueous H-cell and (B) GDE half-cell.

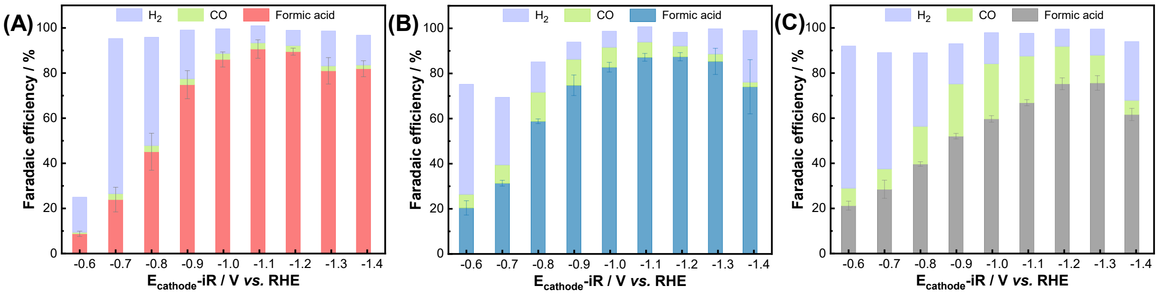

Figure S4. Product distribution for (A) Bi_2O_3, (B) In_2O_3, and (C) SnO_2 in H-cell.

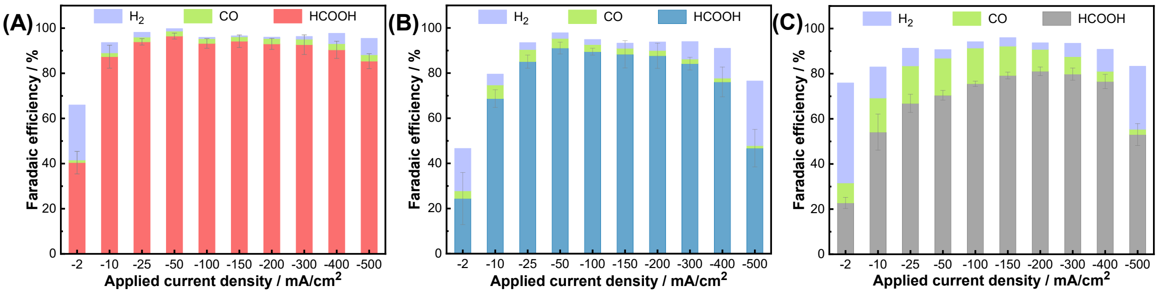

Figure S5. Product distribution for (A) Bi_2O_3, (B) In_2O_3, and (C) SnO_2 in GDE half-cell.

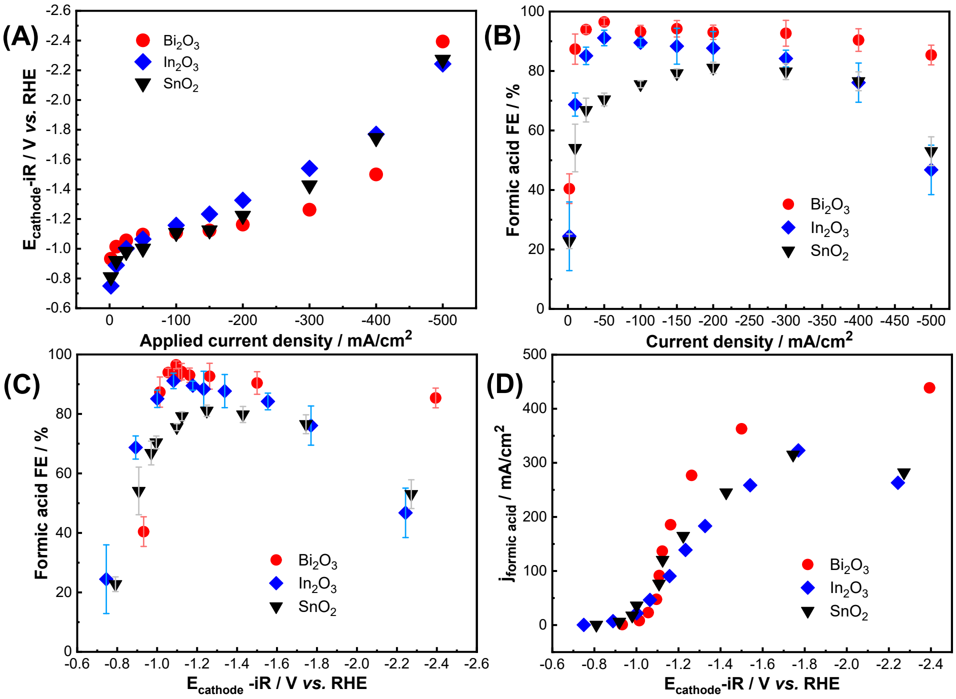

Figure S6. (A) GDE half-cell polarization curve for Bi, Sn, and In oxide catalysts showing the iR-corrected cathode potential ($E_{cathode}$-iR) versus the total applied current density. (B) Formic acid FE and partial current density as a function of total applied current density. (C, D) Formic acid FE and partial current density as a function of $E_{cathode}$-iR.

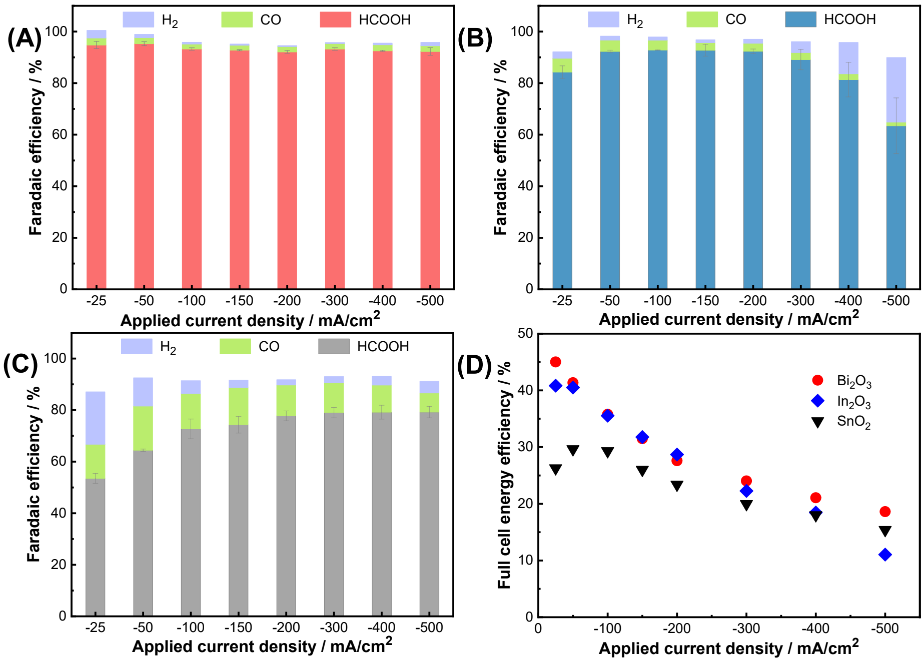

Figure S7. Product distribution of (A) Bi_2O_3, (B) In_2O_3 and (C) SnO_2 GDEs tested in full single gap electrolyzer. (D) Corresponding full energy efficiency for formic acid for all three catalysts.

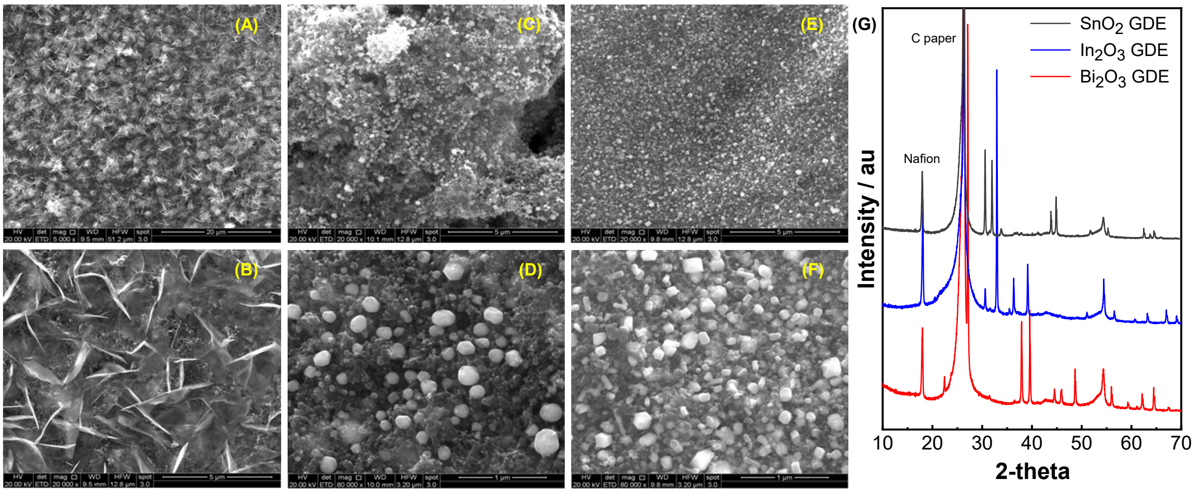

Figure S8. Post electrolysis SEM images of (A, B) Bi_2O_3, (C, D) In_2O_3 and (E, F) SnO_2 GDEs after full cell testing showing significant morphological changes, including SnO_2 and In_2O_3 particle agglomeration and transformation of Bi_2O_3 into 2D-like sheets. (G) Post-mortem XRD pattern after full cell electrolysis showing the dominance of metallic In, Sn, and Bi crystal phase.

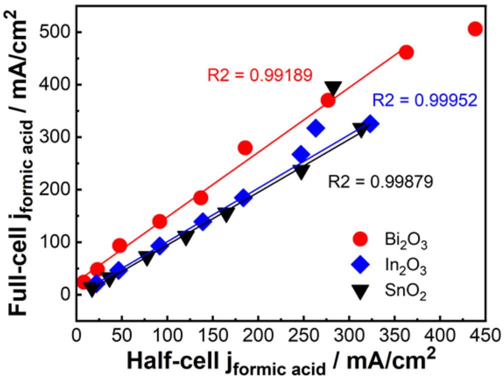

Figure S9. Correlation between half-cell partial current density and full cell current density for all three catalysts.

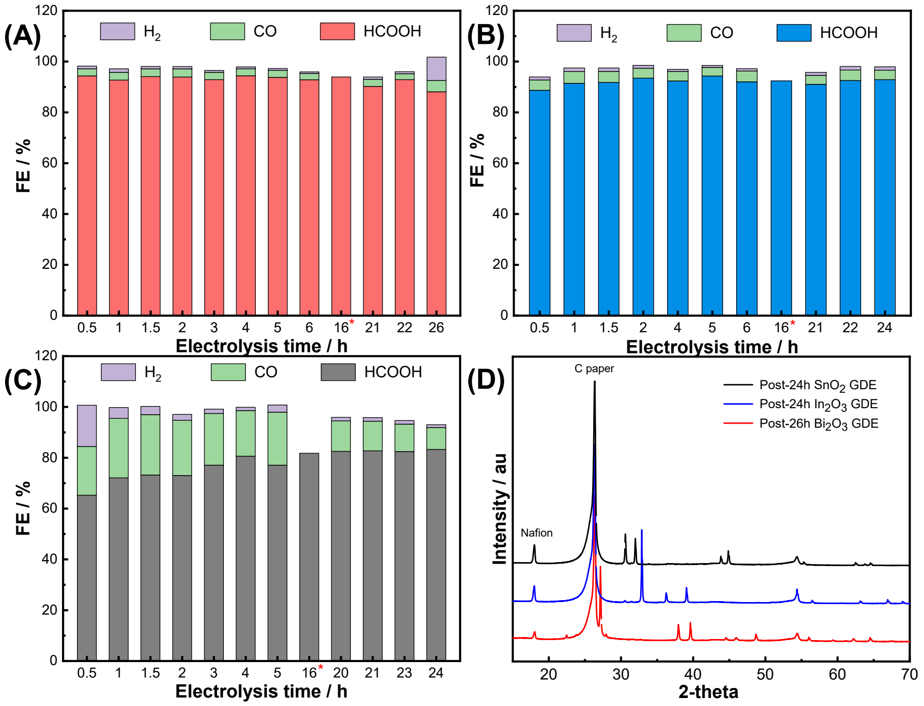

Figure S10. (A-C) Product distribution in stability runs at 100 mA/cm^2 in full cell: (A) Bi_2O_3, (B) In_2O_3, and (C) SnO_2. The asterisks at the 16-h FE data points in (A-C) indicates no gas products were collected during overnight experiment. (D) XRD patterns of GDEs after long-term operation.